Local magnetic susceptibility and electronic structure of the quasi-one-dimensional conductor β-$Na_{0.33}V_2O_5$: ^{51}V NMR study in a single crystal

Tomoyuki Suzuki, Ichihiro Yamauchi, and Masayuki Itoh
Department of Physics, Graduate School of Science, Nagoya University, Furo-cho, Chikusa-ku, Nagoya 464-8602, Japan

Touru Yamauchi and Yutaka Ueda
Institute for Solid State Physics, University of Tokyo, Kashiwanoha, Kashiwa 277-8581, Japan

(Received 6 October 2005; revised manuscript received 1 February 2006; published 15 June 2006)

^{51}V NMR measurements on a single crystal of β-$Na_{0.33}V_2O_5$ have been made to study the local magnetic susceptibility and the electronic structure at the vanadium sites, which provide important information on the metal-insulator transition and the charge ordering, in β-$Na_{0.33}V_2O_5$. We determine in detail the ^{51}V Knight shift and the electric field gradient tensors at the vanadium sites in both the metallic and the insulating phases. We also obtain the temperature dependence of principal components of the ^{51}V Knight shift and the electric field gradient tensors at the vanadium sites. Local magnetic susceptibilities at the V sites are estimated from bulk magnetic susceptibility and the ^{51}V Knight shifts. We conclude that the V1 site has the largest $3d$ local magnetic susceptibility among the three vanadium sites in the metallic state. Electron densities at the three vanadium sites are also discussed and a model of the electronic structure to understand magnetic and electronic properties of β-$Na_{0.33}V_2O_5$ is proposed.

DOI: 10.1103/PhysRevB.73.224421 PACS number(s): 76.60.Cq, 76.60.Gv, 71.30.+h

I. INTRODUCTION

Complex phenomena due to spin, charge, and orbital degrees of freedom have attracted much attention in transition metal oxides.[1] Among them, the charge ordering (CO) is one of the most interesting phenomena in physics related to the charge degrees of freedom. The CO in α'-NaV_2O_5 has been most intensively investigated from experimental and theoretical aspects in mixed-valence vanadium oxides.[2] The ordering with a zigzag pattern was explained as the CO in a quarter-filled ladder system on the trellis lattice.[3] Recently, a series of vanadium bronzes β-$A_{0.33}V_2O_5$ (A=Li,Na,Ca,Sr,Ag,$\cdots$) have renewed interest as candidates to study the CO physics. β-$Na_{0.33}V_2O_5$, a mixed-valence oxide of V^{4+} ($3d^1$) and V^{5+} ($3d^0$), is a typical example among them.[4,5] This oxide undergoes successive phase transitions, namely, an order-disorder transition of Na atoms at $T_{Na}\sim 242$ K, a metal-insulator (MI) transition at $T_{MI}\sim 135$ K where a CO has been considered to take place at the same time, and a transition from a paramagnetic state to an antiferromagnetic (AF) one with canted moments at $T_N\sim 24$ K.[4–6] Recently superconductivity was found to appear at high pressures around 8 GPa below ~ 9 K.[5,7] This superconductivity has attracted much attention from the aspect of a novel superconducting mechanism due to charge fluctuations.

β-$Na_{0.33}V_2O_5$ has a monoclinic structure (the lattice symmetry $C2/m$) at room temperature[8] as is presented in Fig. 1. There are three vanadium sites, V1, V2, and V3. The V1 and V3 sites form zigzag chains along the b axis by sharing the edges of VO_6 octahedra and VO_5 pyramids, respectively, whereas the V2 sites form two-leg ladders along the b axis by sharing the corners of VO_6 octahedra. Na atoms, which are located in a tunnel of the V_2O_5 framework, occupy the A1 sites. The two nearest-neighbor A1 sites are too close to be simultaneously occupied by Na atoms. This leads to the stoichiometric concentration of $x=1/3$ in the β structure. Consequently the nominal ratio of V^{4+} to V^{5+} is 1:5. If V^{4+} is located at the V1 or V3 sites, this oxide is a quarter-filled zigzag chain system. It is a quarter-filled two-leg ladder one, if V^{4+} occupies the V2 sites. Recently, however, based on extended Hückel tight-binding calculations, Doublet and Lepetit proposed weakly interacting two-leg ladders, V1-V3 and V2-V2, as a model of an electronic structure of β-$A_{0.33}V_2O_5$ (A=Ca,Sr,Na,$\cdots$) in contrast with the model with two zigzag chains and a two-leg ladder.[10] Then the average filling of these ladders is one electron for six V sites.

The MI transition has been considered to be accompanied by the CO in β-$Na_{0.33}V_2O_5$. Up to now several models have

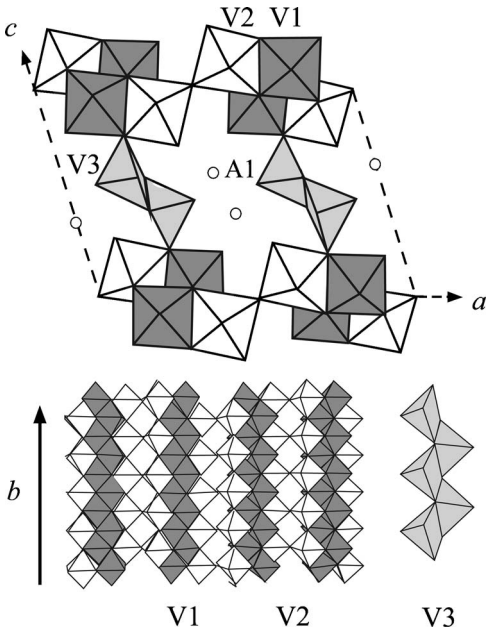

FIG. 1. Crystal structure of β-$Na_{0.33}V_2O_5$ (Ref. 9).

been proposed as the CO pattern in β-$Na_{0.33}V_2O_5$. In previous NMR studies of β-$Na_{0.33}V_2O_5$, we proposed the chain models where V^{4+} are located at half of the V1 or V2 sites, and the zigzag model of V^{4+} located at half of the V2 ladder sites.[9,11] Nishimoto and Ohta showed from the Madelung potential calculations that the V1 sites are occupied by the V^{4+} ions.[12] After these studies Yamaura *et al.* observed the satellite reflections of $\mathbf{q}=\frac{1}{2}\mathbf{b}^*$ due to the Na ordering below T_{Na} and the $\mathbf{q}=\frac{1}{6}\mathbf{b}^*$ below T_{MI} by x-ray diffraction measurements.[13] They proposed a rectangle type of charge ordering with every V site on the V2 ladder. On the other hand, Heinrich *et al.* concluded that 3*d* electrons are located on the V1 zigzag chains from ESR measurements.[14] Photoemission spectroscopy suggested the V1, V2, or simultaneously both sites are occupied by *d* electrons.[15] Recently Nagai *et al.* found by the neutron scattering measurements that the amplitudes of the magnetic moments at the V sites in the three types of V-O chains are modulated with a period of 3*b* along the *b* axis below T_N.[16] They proposed that the charge disproportionation occurs with a period of 3*b*, not 6*b*, and that the 6*b* lattice modulation below T_{MI} is attributed to an instability in the V 3*d* band to form 3*b* charge modulation on the pre-existent 2*b* lattice modulation.

As mentioned above, the CO pattern is controversial. Thus it is highly desirable to clarify how 3*d* electrons are located at the three V sites. NMR is a fruitful technique to study local magnetic and electric properties of a system with several magnetic sites. In particular the Knight shift *K* and the electric field gradient (EFG) tensors are useful to know the local symmetry, local magnetic properties, and electron orbital at the vanadium sites. In the previous NMR studies of β-$Na_{0.33}V_2O_5$, no sample rotation in a magnetic field and partial misorientation of many single crystals stacked parallel to the *b* axis prevented us from knowing precisely *K* and EFG tensors.[9,11] In the present study we have made ^{51}V NMR measurements on a small single crystal with high quality to precisely investigate local magnetic susceptibilities and the electron density in β-$Na_{0.33}V_2O_5$. We determine in detail the *K* and the EFG tensors at the V sites. The temperature *T* dependence of the *K* tensor components, the electric quadrupole frequency ν_Q, and the asymmetry parameter of the EFG η at the vanadium sites is also presented. From the analysis of the ^{51}V Knight shifts at the V sites and the bulk magnetic susceptibility, we obtain local susceptibilities at the three V sites particularly in the metallic phase. We conclude that the V1 site is the most magnetic among the three V sites in the metallic phase. The electron number at the V sites will be discussed. A model of the electronic structure will be also proposed as a framework to explain electronic and magnetic properties of the metallic state in β-$Na_{0.33}V_2O_5$.

II. EXPERIMENTAL PROCEDURE

Single crystals of β-$Na_{0.33}V_2O_5$ were prepared by an rf heating Czochralski method using $NaVO_3$ as a solvent in a Pt crucible.[5] A crystal of $0.5\times2.8\times0.9$ mm^3 was used for the present NMR measurements. NMR measurements were made by using a coherent pulsed spectrometer and a superconducting magnet with a constant field of $H_0=5.8710$ T. Fourier-transformed (FT) NMR spectra for spin-echo signals were measured with the sample rotated in the field. Cu and Ag NMR coils were used for measurements at 300 K and low temperatures, respectively. The Knight shift *K* was determined by using a relation $K=(\nu_{res}-\nu_0)/\nu_0$ where ν_{res} and ν_0 (=65.706 MHz) are ^{51}V resonance frequencies in β-$Na_{0.33}V_2O_5$ and aqueous $NaVO_3$ solution, respectively. In this procedure a contribution of the chemical shift to *K* can be subtracted.

Since the results in the next section are obtained from analyzing in detail NMR spectra, it will be useful to summarize the basic formula used in the next section. The Hamiltonian of a ^{51}V nucleus with the nuclear spin $\mathbf{I}$ ($^{51}I=7/2$) and the nuclear gyromagnetic ratio γ_n at a vanadium site in β-$Na_{0.33}V_2O_5$ is expressed as

$$H=-\gamma_n\hbar\,\mathbf{I}\cdot(1+\mathbf{K})\cdot\mathbf{H_0}+\sum_{\alpha\beta}V_{\alpha\beta}Q_{\alpha\beta}, \tag{1}$$

where $\hbar$ is the Plank's constant, the first term is the Zeeman interaction due to the external field $\mathbf{H_0}$ and the Knight shift tensor $\mathbf{K}$, and the second is the electric quadrupole interaction between the EFG tensor $V_{\alpha\beta}$ and the nuclear quadrupole moment $eQ_{\alpha\beta}$. The electric quadrupole interaction leads to seven lines, namely, one central and six satellite ones, in the ^{51}V NMR spectrum.

One should make NMR experiments with the sample rotated in H_0 to determine the *K* and EFG tensors. We will consider the case of $H_0\perp a^*$, the axis perpendicular to the *b* and *c* axes in the monoclinic structure, and measure the angle of H_0 rotation θ_{a^*} in the *bc* plane from the position in which the *b* axis coincides with H_0. In the first-order perturbation where the electric quadrupole interaction is much smaller than the Zeeman one, the difference between resonance frequencies of the $m\leftrightarrow m-1$ and $-(m-1)\leftrightarrow -m$, $(m=-I+1,\cdots,+I)$, satellite lines $\delta\nu_{m\leftrightarrow m-1}$ is expressed as[17]

$$\delta\nu_{m\leftrightarrow m-1}=\left(m-\tfrac{1}{2}\right)(k_{1,a^*}+k_{2,a^*}\cos 2\theta_{a^*}+k_{3,a^*}\sin 2\theta_{a^*}) \tag{2}$$

with

$$k_{1,a^*}=\nu_Q(V_{bb}+V_{cc})/V_{ZZ},$$

$$k_{2,a^*}=\nu_Q(V_{bb}-V_{cc})/V_{ZZ},$$

$$k_{3,a^*}=-2\nu_Q V_{bc}/V_{ZZ}, \tag{3}$$

and

$$\nu_Q=\frac{3eQV_{ZZ}}{2I(2I-1)h}, \tag{4}$$

where ν_Q is the electric quadrupole frequency, $V_{\alpha\beta}$ (α, $\beta=a^*$, *b*, and *c*) are components of the EFG tensor, V_{ZZ} is the *Z* principal component of the tensor, and $eQ=eQ_{ZZ}$. Similar relations for the H_0 rotations in the ca^* and a^*b planes are obtained by cyclic permutation. In this procedure one can subtract the *K* term as is seen in Eq. (2). After determining the EFG tensor components in the a^*bc coordinate system by using Eqs. (2)–(4), one can obtain the *X*, *Y*, and *Z* principal

components and the principal axes X_Q,Y_Q, and Z_Q by diagonalizing the EFG tensor. The principal components and axes are useful to know the local symmetry at the vanadium sites. Also one can determine ν_Q and $\eta=|V_{XX}-V_{YY}|/|V_{ZZ}|$ ($|V_{XX}|\leq|V_{YY}|\leq|V_{ZZ}|$).

If the second-order electric quadrupole effect is negligibly small, the angular dependence of the central line $\nu_{1/2\leftrightarrow-1/2}$ is determined by the K tensor. In the principal $X_KY_KZ_K$ coordinate system of the K tensor, $\nu_{1/2\leftrightarrow-1/2}$, is expressed as[18]

$$\nu_{1/2\leftrightarrow-1/2}=\nu_0\{(1+K_X)\sin^2\theta\cos^2\phi+(1+K_Y)\sin^2\theta\sin^2\phi+(1+K_Z)\cos^2\theta\}, \quad (5)$$

where K_X, K_Y, and K_Z are the principal components of the K tensor, and $\nu_0=\gamma_n H_0/2\pi$. The θ and ϕ are the polar and azimuthal angles, respectively, between H_0 and the principal axes of the K tensor. The anisotropy of the K tensor particularly provides information of an electron orbital at the V sites. In general it should be noted that X_K, Y_K, and Z_K do not coincide with X_Q, Y_Q, and Z_Q.

III. EXPERIMENTAL RESULTS

We observed ^{51}V NMR spectra coming from the three V sites at 300 K. Figure 2 shows FT spectra with H_0 parallel to the a^*, b, and c axes in β-$Na_{0.33}V_2O_5$. As is seen in Fig. 2, each of two sets of V NMR spectra denoted by S1 and S2 has one central and six satellite lines due to the electric quadrupole interaction, whereas a short nuclear spin-spin relaxation time T_2 prevented us from clearly observing satellite lines in the S3 spectrum. A fact that the intensity of the central line is the weakest in the S1 spectrum for $H_0\|b$ may be due to an indirect interaction due to the Suhl–Nakamura interaction.[19] The spectra are similar to the previous spectra and the notations of the spectra S1–S3 coincide with those in the previous studies.[9,11]

In order to determine the K and EFG tensors at the V sites, we measured the angular dependence of the ^{51}V resonance frequency ν_{res} with H_0 rotated in the ca^*, a^*b, and bc planes for the S1 and S2 spectra at 300 K as demonstrated in Fig. 3. On the other hand, the short T_2 prevented us from clearly observing the angular dependence of ν_{res} for S3. In the present case the electric quadrupole interaction is small enough to be taken into account in the first-order perturbation theory. The experimental results of the angular dependence of ν_{res} were well fitted by using Eqs. (2)–(5). Thus we obtained values of K_X, K_Y, K_Z, ν_Q, and η for the S1 and S2 spectra as listed in Table I. The principal axes of the K and EFG tensors are presented in Figs. 4(a) and 4(b) for S1 and S2, respectively. The principal axes of both the tensors, which coincide and are denoted by $X_{K,Q}$, $Y_{K,Q}$, and $Z_{K,Q}$, are the b, c, and a^* axes, respectively, in the S1 spectrum. On the other hand, the axes of the K and the EFG tensors are different from each other in the S2 spectrum.

We observed the T dependence of the ^{51}V NMR spectra in β-$Na_{0.33}V_2O_5$. Figure 5 shows FT NMR spectra at 300, 150, and 105 K with $H_0\|b$. The S3 spectra were not observed at 150 and 105 K. Two sets of ^{51}V NMR spectra denoted by S1 and S2 were clearly observed at 300 K as mentioned above. At 150 K, the S1 spectrum is split into two spectra of $S1_a$ and $S1_b$ as seen in Fig. 5. On the other hand, we observed no splitting of the S2 spectrum and no reduction of the spectrum intensity at 150 K. At 105 K below T_{MI}, we observed the spectra of $S1_a$ and $S1_b$, and found that the S2 spectrum is split into $S2_a$ and $S2_b$ as seen in Fig. 5. It should be noted that the four spectra denoted by S_a–S_d were observed in addition to these spectra. Comparing the previous NMR results of β-$Na_{0.33}V_2O_5$ with the present spectra, the overall spectra are similar to the previous ones.[9,11] However, we mistook the assignment of the spectra, that is, the $S2_a$ and $S2_b$ spectra in the previous studies are the S_a and S_b spectra in the present spectra. Also we could not observe the S3 spectrum in the paramagnetic insulating phase observed previously below ~40 K maybe because of the short T_2.

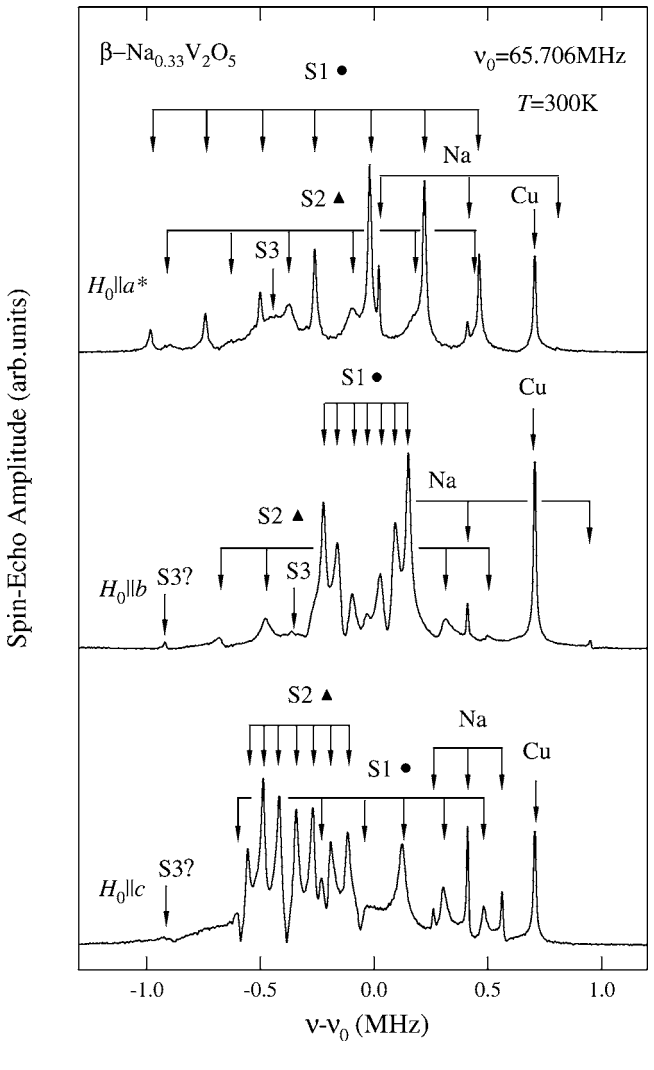

FIG. 2. (a) FT NMR spectra at 300 K with H_0 (=5.8710 T) parallel to the a^*, b, and c axes in β-$Na_{0.33}V_2O_5$. ν_0 (=65.706 MHz) is the ^{51}V resonance frequency in aqueous $NaVO_3$ solution. The symbols of S1, S2, and S3 denote ^{51}V NMR spectra, whereas the symbols of Na represent ^{23}Na NMR spectra. The symbols of Cu are ^{63}Cu spectra in a Cu coil. The arrows represent resonance frequencies of the NMR spectra split by an electric quadrupole interaction.

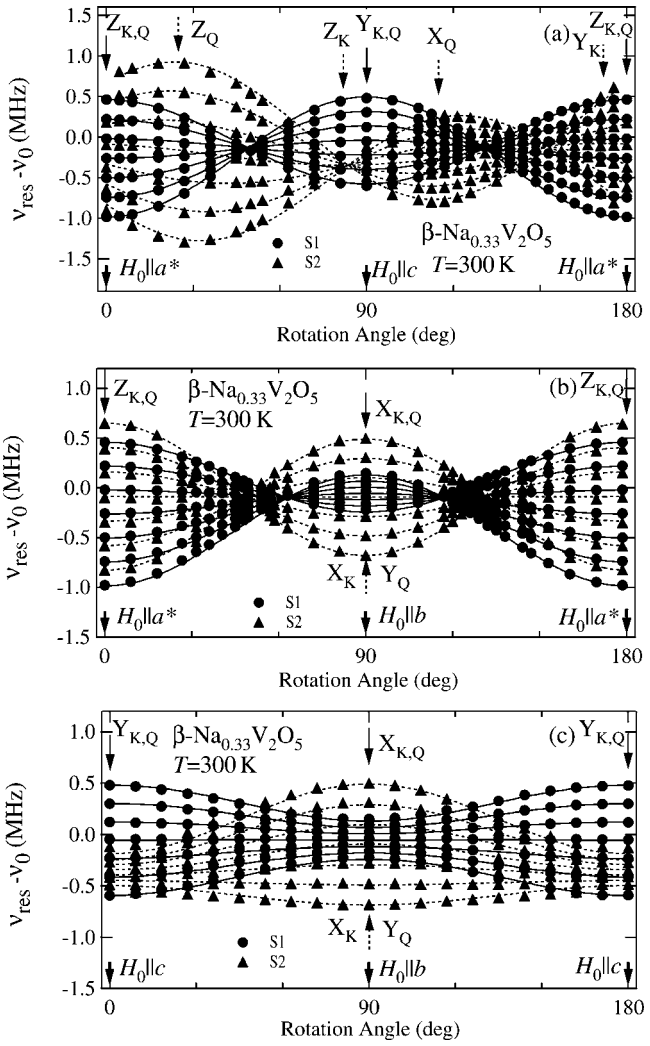

FIG. 3. Angular dependence of the ^{51}V resonance frequency ν_{res} at 300 K with H_0 (=5.8710 T) rotated in the (a) ca^*, (b) a^*b, and (c) bc planes for the S1 and S2 NMR spectra of β-$Na_{0.33}V_2O_5$. ν_0 (=65.706 MHz) is the ^{51}V resonance frequency in aqueous $NaVO_3$ solution. The solid and dotted curves are the fitted results with the parameter values (see Table I) of the K and EFG tensors (see the text). The symbols of $X_{K,Q}$, $Y_{K,Q}$, and $Z_{K,Q}$ with the solid arrows represent the X, Y, and Z principal axes, respectively, of both the Knight shift and EFG tensors in the S1 spectrum. On the other hand, X_K (X_Q), Y_K (Y_Q), and Z_K (Z_Q) with the dotted arrows are the X, Y, and Z principal axes, respectively, of the Knight shift (EFG) tensor in the S2 spectrum.

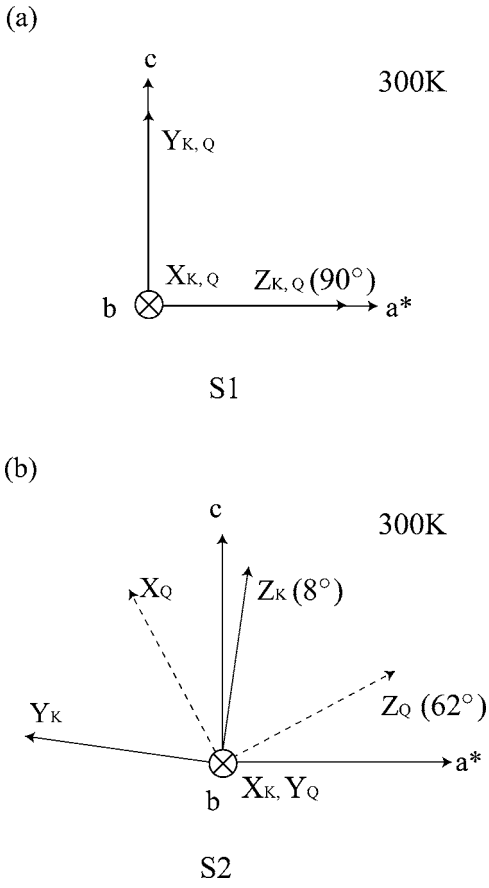

FIG. 4. X, Y, and Z axes of the K and EFG tensors of (a) S1 and (b) S2 NMR spectra at 300 K in β-$Na_{0.33}V_2O_5$. The symbols of $X_{K,Q}$, $Y_{K,Q}$, and $Z_{K,Q}$ are the principal axes for both K and EFG tensors. The X_K, Y_K, and Z_K symbols denote ones for the K tensor, whereas X_Q, Y_Q, and Z_Q represent ones for the EFG tensor. The angles of the $Z_{K,Q}$, Z_K, and Z_Q axes are taken from the c axis in the ca^* plane.

As mentioned above, the ^{51}V NMR spectra drastically change at T_{MI}. In order to determine the EFG and K tensors in the insulating phase of β-$Na_{0.33}V_2O_5$, we measured the angular dependence of ν_{res} at 105 K. The experimental results with H_0 rotated in the ca^* and a^*b planes are presented in Figs. 6(a) and 6(b), respectively. For rotation of H_0 in the ca^* plane, we could determine the angular dependence of ν_{res} for the $S1_a$, $S1_b$, $S2_a$, and $S2_b$ spectra in the wide range of the rotation angle. On the other hand, in the a^*b plane, we observed complicated spectra having many lines. Therefore we could determine only the angular dependence of $S1_a$ and $S1_b$ in the wide angular range, whereas the angular variation of $S2_a$, $S2_b$, and S_a–S_d was done mainly around $H\|b$. The other resonance frequencies we could not assign are omitted in Fig. 6. Since we could not obtain the angular dependence of S_a–S_d in the wide range of the rotation angle, we could not conclude which spectra of S1, S2, and S3 lead to the S_a–S_d spectra. Also the partial missing of the $S1_a$, $S1_b$, $S2_a$,

TABLE I. Knight shift components K_X, K_Y, and K_Z, the electric quadrupole frequency ν_Q, and the asymmetry parameter of the EFG η for the S1 and S2 spectra at 300 K in β-$Na_{0.33}V_2O_5$.

Spectrum	K_X (%)	K_Y (%)	K_Z (%)	ν_Q (MHz)	η
S1	−0.063	−0.086	−0.401	0.241	0.485
S2	−0.124	−0.144	−0.529	0.364	0.071

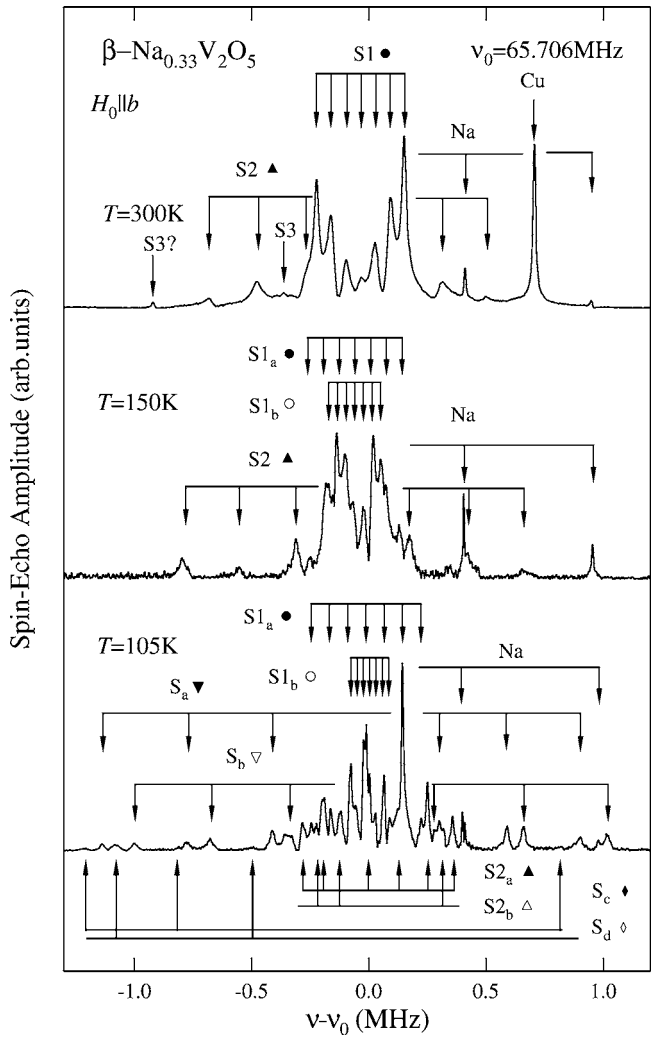

FIG. 5. FT NMR spectra at 300, 150, and 105 K with H_0 (=5.8710 T) parallel to the b axis in β-$Na_{0.33}V_2O_5$. ν_0 (=65.706 MHz) is the ^{51}V resonance frequency in aqueous $NaVO_3$ solution. The symbols of S1, S2, S3, $S1_a$, $S1_b$, $S2_a$, $S2_b$, and S_a–S_d denote the ^{51}V NMR spectra, whereas the symbols of Na and Cu represent the ^{23}Na NMR spectra and the ^{63}Cu spectrum in a Cu coil, respectively. The arrows represent resonance frequencies of the NMR spectra split by an electric quadrupole interaction.

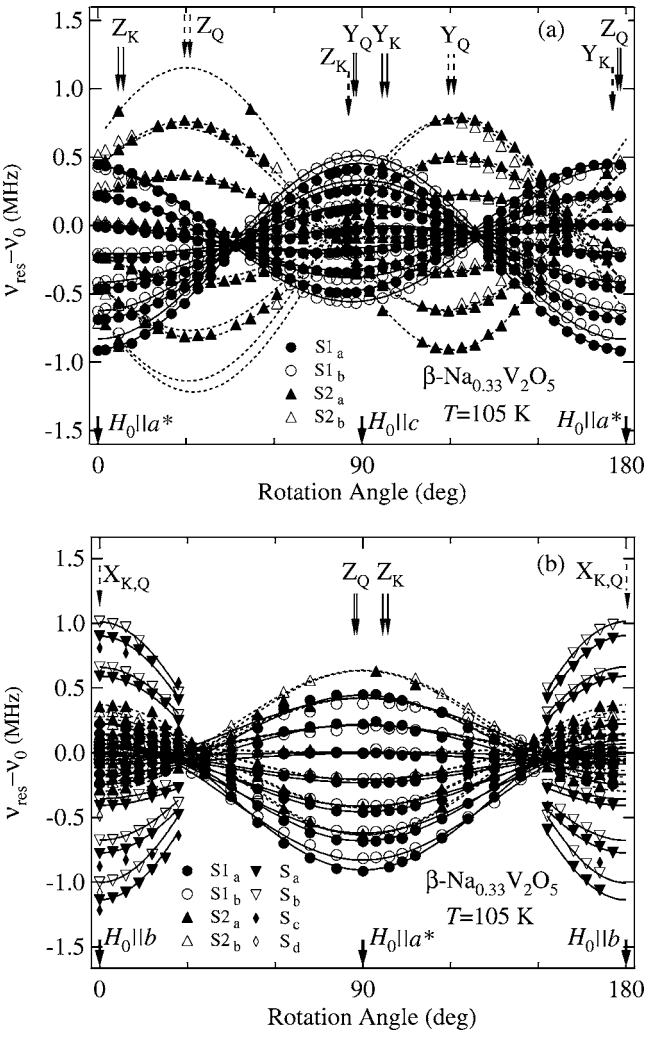

FIG. 6. Angular dependence of the ^{51}V resonance frequency ν_{res} at 105 K with H_0 (=5.8710 T) rotated in (a) the ca^* plane for the $S1_a$, $S1_b$, $S2_a$, and $S2_b$ spectra and (b) the a^*b plane for the $S1_a$, $S1_b$, $S2_a$, $S2_b$, and S_a–S_d spectra of β-$Na_{0.33}V_2O_5$. ν_0 (=65.706 MHz) is the ^{51}V resonance frequency in aqueous $NaVO_3$ solution. The solid and dotted curves for $S1_a$, $S1_b$, $S2_a$, and $S2_b$ are the fitted results with the parameter values (see Table II) of the K and EFG tensors (see the text). The other curves are guides for the eye. The symbols of X_K (X_Q), Y_K (Y_Q), and Z_K (Z_Q) with the solid arrows are the X, Y, and Z principal axes, respectively, of the Knight shift (EFG) tensor in the $S1_a$ and $S1_b$ spectra, while ones with the dotted arrows are in the $S2_a$ and $S2_b$ spectra.

and $S2_b$ spectra taken for the sample rotation in H_0 prevented us from precisely determining the K and the EFG tensors. We fitted the experimental results in Fig. 6 by Eqs. (2)–(5), assuming that the b axis is $X_{K,Q}$, although the $X_{K,Q}$ axis may be deviated from the b axis. Reasonable fitted results as seen in Fig. 6 indicate that the deviation of the $X_{K,Q}$ axis is small. Thus we obtained values of K_X, K_Y, K_Z, ν_Q, and η for $S1_a$, $S1_b$, $S2_a$, and $S2_b$ as listed in Table II. The principal axes are also presented in Fig. 7(a) [Fig. 7(b)] for $S1_a$ and $S1_b$ ($S2_a$ and $S2_b$). In the $S1_a$ and $S1_b$ spectra, the principal axes of both the K and EFG tensors change from the axes at 300 K. The difference between the directions of the axes in $S1_a$ and $S1_b$ is small as well as that in $S2_a$ and $S2_b$.

The T dependence of the Knight shifts is useful to clarify local magnetic susceptibilities of the V sites in β-$Na_{0.33}V_2O_5$. We measured the T dependence of K_X, K_Y, and K_Z for the S1, $S1_a$, and $S1_b$ spectra. The results are shown in Fig. 8(a). To clarify anisotropy of the K tensor, we introduce K_{iso}, K_{ax}, and K_{aniso} expressed as $K_{iso}=(K_X+K_Y+K_Z)/3$, $K_{ax}=(2K_Z-K_X-K_Y)/6$, and $K_{aniso}=(K_Y-K_X)/2$. The T dependence of K_{iso}, K_{ax}, and K_{aniso} is also presented in Fig. 8(b). The overall T dependence of K is the same as that in the previous studies.[9,11] As seen in Fig. 8, the K tensors of S1, $S1_a$, and $S1_b$ have almost axial symmetry in both the metallic and insulating phases. All the principal values of the K tensor show a Curie-Weiss (CW) like behavior above T_{Na}. At T_{Na}, the S1 spectrum is split into the $S1_a$ and $S1_b$ ones. The Knight shifts of both $S1_a$ and $S1_b$ show a CW-like be-

TABLE II. Knight shift components K_X, K_Y, and K_Z, the electric quadrupole frequency ν_Q, and the asymmetry parameter of the EFG η for the $S1_a$, $S1_b$, $S2_a$, and $S2_b$ spectra at 105 K in β-$Na_{0.33}V_2O_5$.

Spectrum	K_X (%)	K_Y (%)	K_Z (%)	ν_Q (MHz)	η
$S1_a$	−0.017	−0.055	−0.360	0.226	0.310
$S1_b$	0.007	−0.030	−0.316	0.209	0.699
$S2_a$	0.054	0.001	−0.142	0.395	0.435
$S2_b$	0.066	0.001	−0.128	0.370	0.511

havior in the T range $T_{MI} \leq T \leq T_{Na}$. At T_{MI}, a jump is seen in all K components. Below T_{MI}, the absolute values of K_{iso} and K_{ax} have a broad peak around 100 K and decrease with decreasing T. On the other hand, the T dependence of K_X, K_Y, and K_Z for S2, $S2_a$, and $S2_b$ is presented in Fig. 9(a). Also Fig. 9(b) shows the T dependence of K_{iso}, K_{ax}, and K_{aniso}. The S2 spectrum is not split at T_{Na} and is split into the $S2_a$ and $S2_b$ spectra at T_{MI}. It should be noted that K_{iso} changes from a CW-like behavior to a T independent behavior like Pauli paramagnetism at T_{Na} with decreasing T. At T_{MI}, the absolute value of K_{iso} drastically decreases and goes to zero with decreasing T. The T dependence of the Knight shifts for the S_a–S_d spectra with $H_0 \| b$ below T_{MI} is presented in Fig. 10 where the T dependence of K_X for the S2, $S2_a$ and $S2_b$ spectra is also included. These Knight shifts were determined from the satellite lines. The S_c and S_d spectra have the largest negative Knight shifts among three groups of the NMR spectra as seen in Fig. 10.

Figure 11(a) shows the T dependence of ν_Q and η for the S1, $S1_a$, and $S1_b$ spectra. As seen in Fig. 11(a), both ν_Q and η of S1 are split at T_{Na}. The ν_Q of $S1_a$ gradually increases and η of $S1_a$ decreases with decreasing T below T_{Na}, while ν_Q of $S1_b$ gradually decreases and η of $S1_b$ increases below T_{Na}. Below T_{MI}, ν_Q of $S1_a$ is almost T independent after a small jump at T_{MI} and η of $S1_a$ shows weak T dependence after drastic reduction at T_{MI}. The ν_Q of $S1_b$ gradually decreases and becomes T independent with decreasing T, whereas η of $S1_b$ gradually increases with decreasing T. On

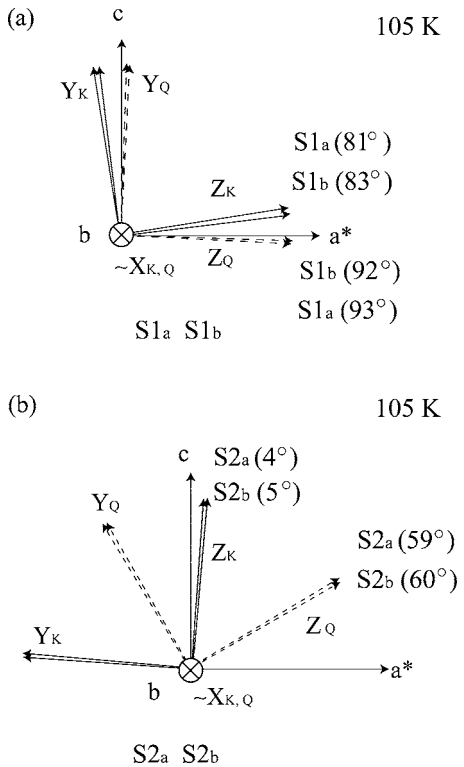

FIG. 7. X, Y, and Z axes of the K and EFG tensors of (a) $S1_a$, $S1_b$, (b) $S2_a$, and $S2_b$ NMR spectra at 105 K in β-$Na_{0.33}V_2O_5$. The symbols of X_K, Y_K, and Z_K denote the principal axes for the K tensor, whereas X_Q, Y_Q, and Z_Q represent ones for the EFG tensor. The $X_{K,Q}$ symbol is the X axis for both K and EFG tensors. The angles of the Z_K and Z_Q axes are taken from the c axis in the ca^* plane.

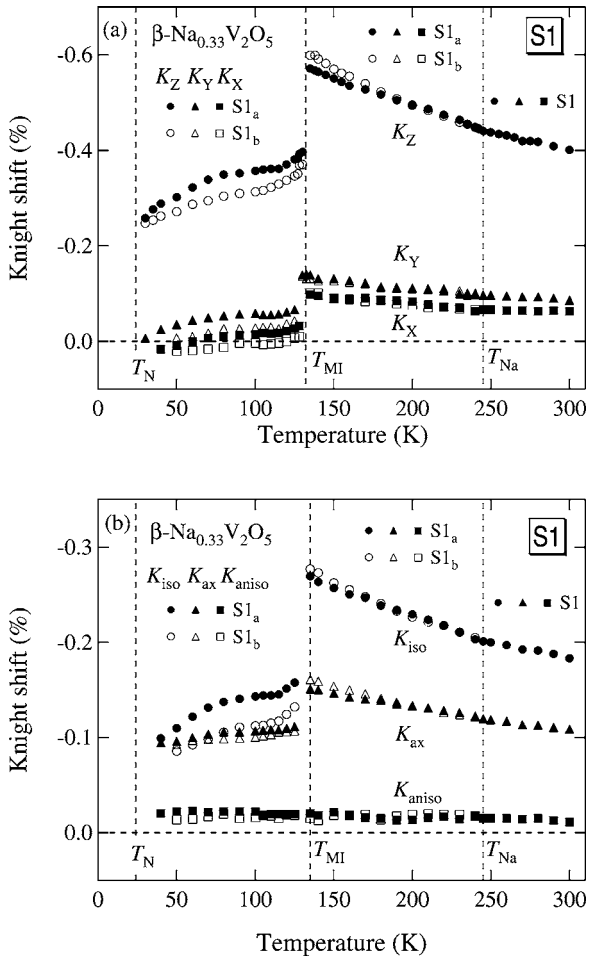

FIG. 8. Temperature dependence of the ^{51}V Knight shifts (a) K_X, K_Y, K_Z, (b) K_{iso}, K_{ax}, and K_{aniso} for the S1 spectrum above T_{Na}, and the $S1_a$ and $S1_b$ spectra below T_{Na} in β-$Na_{0.33}V_2O_5$.

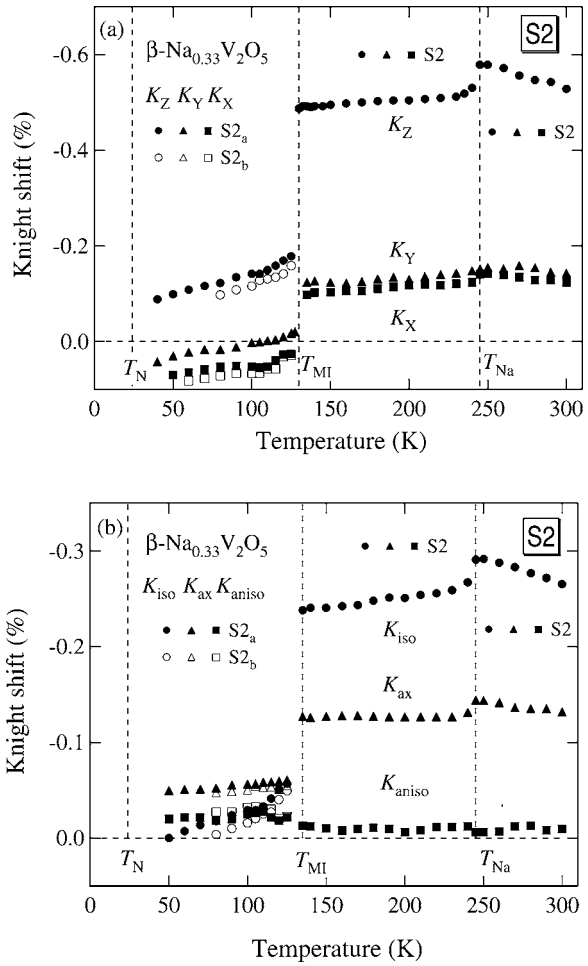

FIG. 9. Temperature dependence of ^{51}V Knight shifts (a) K_X, K_Y, and K_Z, and (b) $K_{\rm iso}$, $K_{\rm ax}$, and $K_{\rm aniso}$ for the S2 spectrum above $T_{\rm MI}$, and the S2$_a$ and S2$_b$ spectra below $T_{\rm MI}$ in β-Na$_{0.33}$V$_2$O$_5$.

the other hand, Fig. 11(b) shows the T dependence of ν_Q and η for the S2, S2$_a$, and S2$_b$ spectra. The ν_Q and η of S2 are not split and have a jump at $T_{\rm Na}$. Both ν_Q and η are split at $T_{\rm MI}$. The ν_Q of S2$_a$ gradually increases and ν_Q of S2$_b$ decreases with decreasing T below $T_{\rm MI}$. Both η of S2$_a$ and S2$_b$ increase and become T independent with decreasing T.

IV. ANALYSIS AND DISCUSSION

A. NMR spectrum and vanadium site

We first discuss the number of the V sites observed by the present NMR experiments, comparing those with the crystallographic V sites. X-ray and neutron scattering measurements proposed the crystal symmetry of β-Na$_{0.33}$V$_2$O$_5$ is $C2/m$ above $T_{\rm Na}$ and $P2_1/a$ below $T_{\rm Na}$.[13,16] Figures 12(a)–12(c) show, for example, the projection of the V3 sites on the bc plane in the T range, $T>T_{\rm Na}$, $T_{\rm MI}\leq T\leq T_{\rm Na}$, and $T<T_{\rm MI}$, respectively. Mirror planes, glide planes, twofold screw axes, twofold rotation axes, and inversion centers are also presented.[16,20]

Above $T_{\rm Na}$, there is crystallographically inequivalent one V3 site as seen in Fig. 12(a) where the numbers represent the

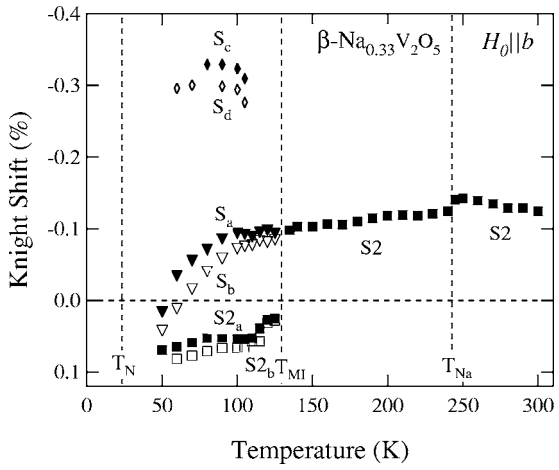

FIG. 10. Temperature dependence of ^{51}V Knight shifts of the S$_a$, S$_b$, S$_c$, and S$_d$ spectra with $H_0\|b$ in β-Na$_{0.33}$V$_2$O$_5$. The Knight shifts K_X of the S2, S2$_a$, and S2$_b$ spectra are included for comparison.

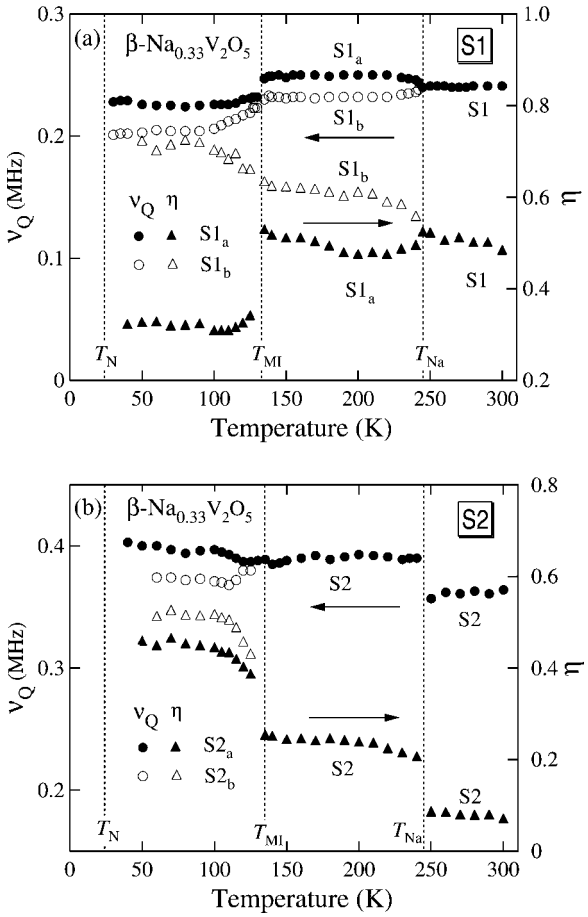

FIG. 11. Temperature dependence of the ^{51}V electric quadrupole frequency ν_Q (solid and open circles) and the asymmetry parameter η (solid and open triangles) of the EFG of (a) the S1 spectrum above $T_{\rm Na}$, the S1$_a$ and S1$_b$ spectra below $T_{\rm Na}$, (b) the S2 spectrum above $T_{\rm MI}$, and the S2$_a$ and S2$_b$ spectra below $T_{\rm MI}$ in β-Na$_{0.33}$V$_2$O$_5$.

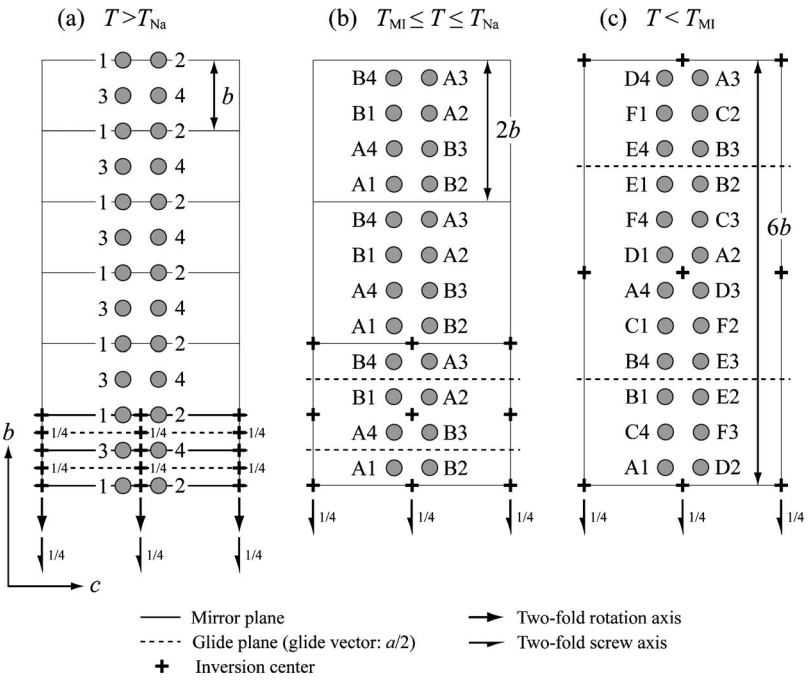

FIG. 12. Projection of the V3 sites on the *bc* plane for (a) $T>T_{Na}$, (b) $T_{MI}\leq T\leq T_{Na}$, and (c) $T<T_{MI}$ in β-$Na_{0.33}V_2O_5$. Mirror planes, glide planes, twofold rotation axes, twofold screw axes, and inversion centers are also presented in the unit cells.

positions of the V3 site in the unit cell. Therefore, there are only three vanadium sites, V1, V2, and V3. This is consistent with observation of only the S1, S2, and S3 NMR spectra.

In the T range $T_{MI}\leq T\leq T_{Na}$, each V site is split into the crystallographically inequivalent two V sites due to the Na ordering as represented by A and B in Fig. 12(b). At the same time, the mirror planes and the twofold rotation axes are lost, whereas the glide planes, twofold screw axes, and inversion centers remain as shown in Fig. 12(b). This fact is expected to result in that the V3($A1$) and V3($A3$) positions may have EFG tensors with different directions from those of V3($A2$) and V3($A4$), because the principal axes of the EFG tensors may tilt from the b axis. However, this was not observed maybe due to the small tilting in the present V NMR spectra. Thus, we take account of only crystallographically inequivalent six V sites, V1A, V1B, V2A, V2B, V3A, and V3B, to understand the observed NMR spectra. We found that the S1 spectrum is split into two spectra $S1_a$ and $S1_b$ at T_{Na}, whereas the S2 spectrum is not split. No reduction of the intensity of the S2 spectrum at T_{Na} clearly shows that the S2 NMR spectrum observed below T_{Na} is composed of the $S2_a$ and $S2_b$ spectra coming from both the two sites expected crystallographically. Thus it is concluded that the V site of $S1_a$ has magnetic and electric properties different from ones of $S1_b$, while electric and magnetic properties of $S2_a$ coincide with ones of $S2_b$. The S3 NMR spectrum was not clearly observed maybe due to the short T_2.

Below T_{MI}, the 6b lattice modulation along the b axis results in the appearance of the crystallographically inequivalent six sites, $A-F$, for each of the V1, V2, and V3 sites as shown in Fig. 12(c).[13,16] Therefore 18 sets of ^{51}V NMR spectra should be observed. In the present NMR experiments, we observed the splitting of the S1 (S2) spectrum to the $S1_a$ and $S1_b$ ($S2_a$ and $S2_b$) ones. In addition to these NMR spectra, four sets of ^{51}V NMR spectra S_a-S_d were observed. Therefore we could not observe 10 sets of NMR spectra, which may come from magnetic sites with a short T_2, among the expected 18 sets, or these spectra may be hidden in the complicated resonance lines which we could not assign. Recently Nagai *et al.* proposed from neutron scattering measurements that magnetic moments in the AF state occupy the B, C, E, and F positions of the V1,V2, and V3 sites, namely 12 V sites, and that each of V1,V2, and V3 sites has two nonmagnetic V^{5+} sites located at A and D positions,in the AF state.[16] They inferred a pattern of the charge disproportionation in the insulating phase based on the spin structure in the AF state. A similar model of the charge disproportionation is proposed by our ^{23}Na NMR results which will appear elsewhere.[21] If so, the $S1_a$, $S1_b$, $S2_a$, and $S2_b$ spectra observed in the T range $T_N\leq T\leq T_{MI}$ are ascribed to nonmagnetic V^{5+} sites of two V sites, which are considered as the V2 and V3 sites from the later discussion, among the V1,V2, and V3 sites. The S_a and S_b spectra may come from the nonmagnetic V^{5+} sites of the other V site which may be the V1 site, whereas two magnetic sites located at the B, C, E, or F positions of the V1, V2, and V3 sites may lead to the S_c and S_d spectra with absolute values of K larger than those of S_a and S_b.

B. Local magnetic susceptibility

We estimate local magnetic susceptibilities of the three V sites in the metallic state from the magnetic susceptibility χ of a powdered sample[9] and ^{51}V Knight shifts in the present NMR experiment. The data of χ above T_{MI} can be well fitted to the CW law as $\chi=C/(T-\Theta)$ with $C=0.0798$ emu K/V mol and $\Theta=-163$ K. Absence of a T-independent term indicates that the orbital susceptibility χ_{iso}^{VV} is small and cancelled by the diamagnetic susceptibility, -3.5×10^{-5} emu/V mol.[22] Therefore χ is expressed as $\chi\sim\Sigma_i\chi_{iso}^{d}(i)/3$ for $T>T_{Na}$ where $\chi_{iso}^{d}(i)$ (i=S1, S2, and S3) is the isotropic d spin susceptibility of the V sites leading to the

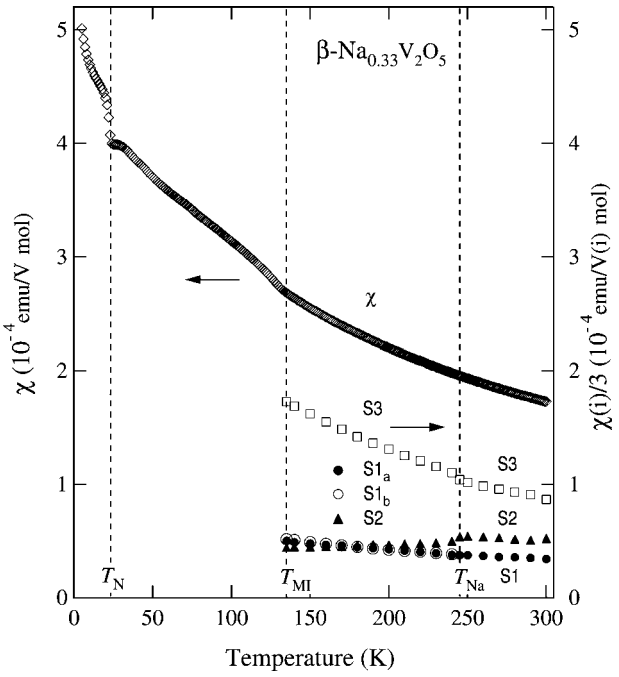

FIG. 13. Temperature dependence of magnetic susceptibility of a powdered sample χ (Ref. 9) and isotropic local magnetic susceptibilities $\chi(i)$ of the V sites leading to the i (=S1,S2,S3,S1$_a$ and S1$_b$) NMR spectra in β-$Na_{0.33}V_2O_5$.

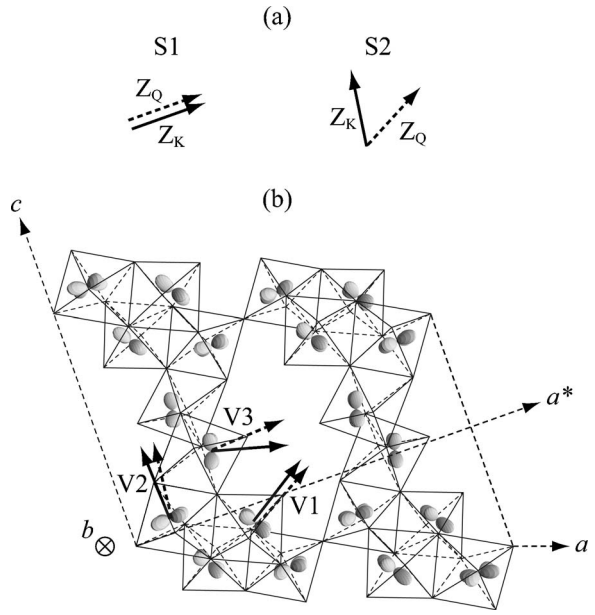

FIG. 14. (a) Experimental and (b) calculated directions of the Z axes of the K (solid arrows) and EFG (dashed ones) tensors at 300 K in β-$Na_{0.33}V_2O_5$. The 3d electron orbitals at the V1, V2, and V3 sites calculated from a crystal field approximation in the point charge model are also shown.

i spectrum, and $\chi \sim \chi^d_{\rm iso}(S1_a)/6+\chi^d_{\rm iso}(S1_b)/6+\chi^d_{\rm iso}(S2)/3+\chi^d_{\rm iso}(S3)/3$ for $T_{\rm MI} \leq T \leq T_{\rm Na}$. On the other hand, the isotropic Knight shift $K_{\rm iso}(i)$ of the i spectrum is expressed as $K_{\rm iso}(i) \sim K^d_{\rm iso}(i)$ where $K^d_{\rm iso}(i)$ is the Knight shift due to $\chi^d_{\rm iso}(i)$, assuming the orbital Knight shift is reasonably neglected due to the small $\chi^{\rm VV}_{\rm iso}$ as will be confirmed later. It should be noted that the chemical shift is subtracted from the definition of the Knight shift. Also $K^d_{\rm iso}(i)$ is expressed as[18]

$$K^d_{\rm iso}(i) = \frac{A^d_{\rm hf}}{N\mu_B}\chi^d_{\rm iso}(i), \tag{6}$$

where $A^d_{\rm hf}$ is the hyperfine coupling constant of the Fermi contact interaction due to the core polarization effect, N is the Avogadro's number, and μ_B is the Bohr magneton. Using a value of $A^d_{\rm hf} \sim -100$ kOe/μ_B for a $3d^1$ system[23] and the present experimental results of $K_{\rm iso}(i)$ (i=S1, S1$_a$, S1$_b$, and S2), we obtain $\chi^d_{\rm iso}(i)$ from Eq. (6). We also obtain $\chi^d_{\rm iso}$(S3) after subtracting $\chi^d_{\rm iso}(i)$ (i=S1, S1$_a$, S1$_b$, and S2) from the experimental data of χ. Thus we can estimate isotropic local magnetic susceptibilities $\chi(i) \sim \chi^d_{\rm iso}(i)$ (i=S1, S1$_a$, S1$_b$, S2, and S3) as presented in Fig. 13. Below $T_{\rm MI}$, we cannot obtain local magnetic susceptibilities of the V sites, because we could not observe all of the S1 and S2 spectra.

Finally, in order to confirm the validity of the present analysis, we estimate the orbital susceptibilities, which were neglected in the above analysis, from the conventional $K_{\rm iso}$ vs $\chi(i)$ plots. Using a value of the orbital hyperfine coupling constant $A^{\rm VV}_{\rm hf}(=2N\mu_B\langle r^{-3}\rangle)=461$ kOe/μ_B where $\langle r^{-3}\rangle$, the average value of r^{-3} for a 3d orbital, is the Hartree-Fock value of 3.684 a.u. for V^{4+},[24] we obtain $\chi^{\rm VV}_{\rm iso}=6.2\times10^{-6}$ emu/V(i) mol for i=S1 and S2. Thus the small value of $\chi^{\rm VV}_{\rm iso}$ shows that the local magnetic susceptibilities obtained in the present analysis are reasonable.

In conclusion, we find that the S3 NMR spectrum comes from the most magnetic V sites in the metallic phase.

C. Site assignment

Next we make a site assignment of the NMR spectra, S1–S3. The anisotropy of the K tensor as shown in Fig. 14(a), where the Z axes of the K and EFG tensors determined experimentally are shown, allows us to know d orbitals at the V sites. We calculate 3d orbitals at the V1, V2, and V3 sites in a crystal field approximation for the $V1O_6$, $V2O_6$, and $V3O_6$ octahedra where the apical oxygen is included for the $V3O_5$ pyramid as shown in Fig. 14(b), because the 3d orbital calculated for the $V3O_6$ octahedron reproduces more suitably the NMR shift tensor than for the $V3O_5$ square pyramid. Using the crystal structure determined by Yamaura *et al.*,[25] we obtained the wave functions at the V1, V2, and V3 sites as $0.542d_{xy}-0.840d_{yz}$, $0.999d_{xy}+0.042d_{yz}$, $0.261d_{xy}+0.965d_{yz}$, respectively, in the xyz (a^*bc) coordinate system. These orbitals shown in Fig. 14(b) are d_{xy}-type ones with an axial symmetry. The 3d orbitals at the V1 and V3 sites are roughly in the bc plane, whereas the 3d orbital at the V2 site is in the a^*b plane. These results come from the local distortion of the highly distorted VO_6 octahedra as discussed in β-$Sr_{0.33}V_2O_5$ by Doublet and Lepetit[10] and in β'-$Cu_xV_2O_5$ by Yamaura *et al.*[26] A Knight shift tensor is well known to be governed by a local 3d orbital. Therefore, the Z_K principal axes of the K tensors should be in the direction of the solid arrows in Fig. 14(b) which are drawn in the ca^* plane as

perpendicular to the d_{xy} type orbitals. The directions of the Z_K axes determined experimentally agree well with the calculated ones as seen in Fig. 14. Also the anisotropy of the d_{xy} type orbitals is consistent with almost the axial symmetry of the K tensors observed in the S1 and S2 spectra. Thus we can conclude that the S1 and S2 NMR spectra come from the V3 and V2 sites, respectively. Also our conclusion that the V1 site is the most magnetic is consistent with the ESR result[14] and the Madelung energy calculation.[12] It should be also noted that the present determination of the Z_K axis in the K tensor is a direct observation of the orbital ordering in β-$Na_{0.33}V_2O_5$.

The EFG tensor also provides information of the local symmetry at the V sites. As is well known, the EFG tensor at a magnetic ion has two contributions from on-site electrons and ions outside the magnetic ion in concern.[18] One can usually calculate the latter contribution in a point charge model. We assume $Na^{0.5+}$ at the $A1$ sites, because half of the Na sites are randomly occupied by Na^+ at 300 K. From the electron density at the V1–V3 sites as will be estimated below, we assume $V^{4.7+}$, $V^{4.8+}$, and $V^{4.9+}$ at the V1, V2, and V3 sites, respectively. This assumption is not sensitive to the calculated direction of the EFG tensor at the V sites. The lattice summation in the EFG calculation was taken over the lattice sites in a sphere with a radius of 200 Å. The calculated directions of the Z_Q axes in the EFG tensors are represented by the dashed arrows in Fig. 14. The on-site electron contribution to the EFG tensor is estimated from the d orbitals at the magnetic ions. That is, the Z_Q axis of the EFG due to this contribution should coincide with Z_K of the K tensor. As seen in Fig. 14, the calculated Z_Q axes due to the contribution of the outside ions for the three V sites have almost the same direction as the calculated Z_K axes. This comes from a fact that the Knight shift and EFG tensors are generally governed by the local symmetry. The calculated Z_Q axis of the EFG tensors at the V3 site almost coincides with the experimental result, whereas the agreement between the calculated and experimental ones is relatively poor at the V2 site. The origin of the poor agreement is not clear at present.

D. Electronic structure

In order to understand the mechanism of the MI transition, it is desired to clarify the electronic structure of the metallic state. For this purpose, first, we roughly estimate the $3d$ electron number at each V site from magnetic susceptibility, although it is generally difficult to determine the electron number from magnetic susceptibility except Pauli paramagnetic susceptibility proportional to the density of states at the Fermi level. Previously the charge disproportionation of the V^{3+} and V^{4+}-like sites in metallic states of vanadium oxides with a strong electron-electron interaction was discussed from local magnetic susceptibilities.[27] Following these studies, we estimate the electron number of the V1-V3 sites from the local magnetic susceptibilities. For $T \geq T_{Na}$, we fit the local magnetic susceptibilities $\chi(V1)-\chi(V3)$ obtained in the present experiments to the CW law with $\Theta=-163$ K, the Weiss temperature of the bulk magnetic susceptibility. We obtain the effective magnetic moment $\mu_{eff}[=2\mu_B\sqrt{S(S+1)}]=0.99$, 0.74, and $0.61\mu_B$ for $\chi(V1)$, $\chi(V2)$, and $\chi(V3)$, respectively. Because the spin S may be proportional to the electron number, the ratio of the $3d$ electron number on the V1, V2, and V3 sites may be about 0.21:0.12:0.09, respectively, for $T \geq T_{Na}$. In β-$Na_{0.33}V_2O_5$, the nominal ratio of V^{4+} to V^{5+} is 1:5. Thus we roughly obtain the $3d$ electron number on the V1, V2, and V3 sites as 0.25, 0.14, and 0.11 electron/V-ion, respectively, above T_{Na}. In the T range $T_{MI} \leq T \leq T_{Na}$, we cannot estimate the local electron numbers, because $\chi(V2)$ changes from the CW to the Pauli paramagnetic behaviors, whereas $\chi(V1)$ and $\chi(V3)$ follow the CW laws below T_{Na} as well as above T_{Na}. However, the $3d$ electron numbers at the three V sites seem not to change drastically at T_{Na}, since $\chi(V2)$ below T_{Na} does not drastically deviate from $\chi(V2)$ extrapolated from the CW law above T_{Na} as seen in Fig. 13.

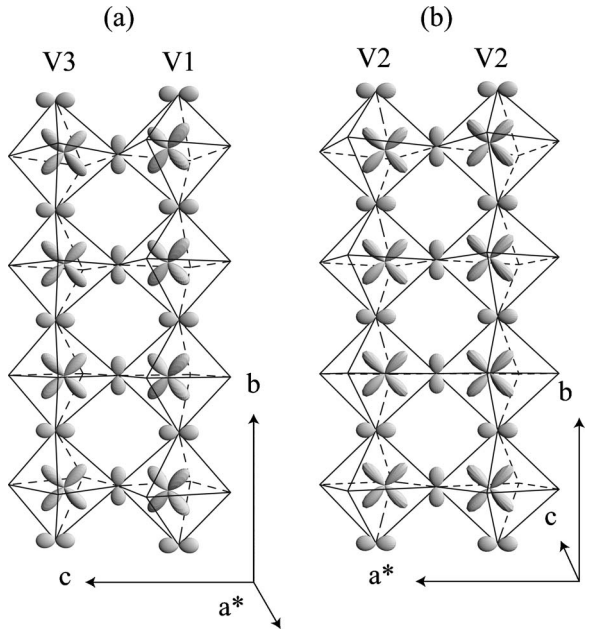

FIG. 15. $3d$ electron orbitals (a) at V1 and V3 sites in a V1-V3 ladder, and (b) at V2 sites in a V2-V2 ladder of β-$Na_{0.33}V_2O_5$. Bridging oxygen $2p$ orbitals are also presented.

As mentioned in the last subsection, the V1, V2, and V3 sites have characteristic d orbitals which are expected to result in anisotropic interactions. Recently, based on vanadyl bond orientation and extended Hückel tight-binding calculations, Doublet and Lepetit calculated a transfer integral between the V atoms in an isomorphous oxide β-$Sr_{0.33}V_2O_5$ and discussed exchange interactions.[10] Following their results, we discuss the electronic and magnetic interactions of β-$Na_{0.33}V_2O_5$. The hopping between the orbitals of the nearest neighboring V1 sites in the V1 zigzag chains is not bridged by any oxygen orbital as seen in Fig. 14(b), resulting in a negligibly small magnetic interaction. On the other hand, the second nearest neighboring V1 sites along the b axis have d orbitals with which a p orbital of a bridging oxygen overlaps as seen in Fig. 15(a), where the $3d$ orbitals at the V1 and V3 sites and the bridging oxygen $2p$ orbitals are presented, leading to a strong magnetic interaction along the b axis. The orbitals at the V3 sites in the V3 zigzag chains have

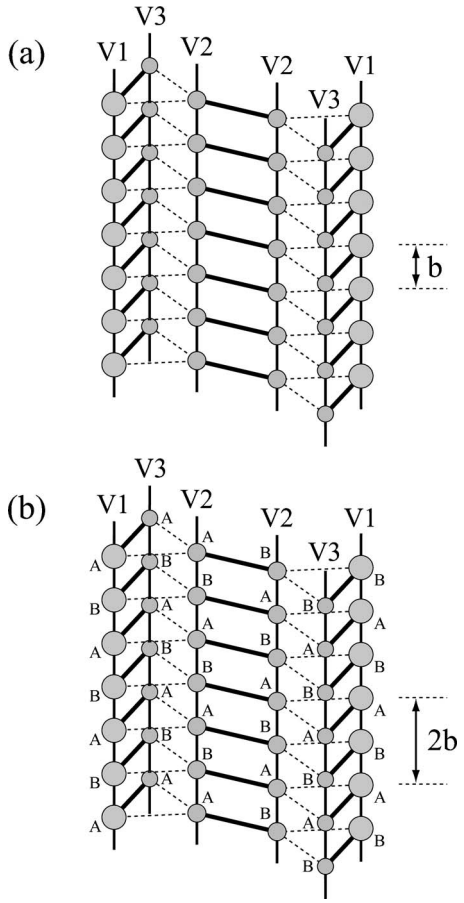

FIG. 16. Schematic structure of dominant interactions and electron number for (a) $T > T_{Na}$ and (b) $T_{MI} \leq T \leq T_{Na}$ in the metallic state of β-$Na_{0.33}V_2O_5$. The ratio of the size of the gray circles corresponds to the ratio of the electron number roughly estimated at the V1, V2, and V3 sites.

characters similar to the orbitals at the V1 sites. It should be noted that another large interaction between the nearest neighboring V1 and V3 sites appears in contrast with the V1 zigzag and the V3 zigzag chains. Thus the nearest V1-V3, the second nearest V1-V1, and the second nearest V3-V3 interactions form the V1-V3 ladders along the *b* axis as presented in Fig. 15(a). The interaction between the nearest neighboring V2 sites in the V2 ladders is strong due to the bridging oxygen overlap as seen in Fig. 15(b). Also the second nearest neighboring V2 sites along the *b* axis have a strong interaction. Thus the nearest and the second nearest V2-V2 interactions form V2-V2 ladders as shown in Fig. 15(b). These V2-V2 and V1-V3 ladders are coupled by weak interactions via bridging oxygen.

Taking account of these results, we propose a model of the electronic structure as shown schematically in Fig. 16 to explain magnetic and electronic properties of the metallic state of β-$Na_{0.33}V_2O_5$. In the weakly coupled ladders composed of one V2-V2 ladder and two V1-V3 ladders, the V1 site has the largest $3d$ electron density among the V1-V3 sites as presented in Fig. 16(a). Above T_{Na}, the electron density is uniform at each V site in the ladders, whereas in the T range $T_{MI} \leq T \leq T_{Na}$ the Na ordering may lead to a slight $2b$ modulation at each V site along the *b* axis as presented by *A* and *B* in Fig. 16(b). The electronic and magnetic interactions in this model agree with those in the model proposed for β-$Sr_{0.33}V_2O_5$ by Doublet and Lepetit who did not discuss the local electron number.[10] However, this disagrees with the V3-V1-V2-V2-V1-V3 cluster model which was proposed by Nagai *et al.* without taking reasonably the V-V interactions via the $3d$ vanadium and the oxygen $2p$ orbitals into account.[16]

The $3d$ orbitals at the V1-V3 sites form the $3d$ band in the metallic state of β-$Na_{0.33}V_2O_5$. The Na ordering at T_{Na} also leads to the change of the magnetic behavior. The local magnetic susceptibility of the V2 site changes from the CW-like behavior to the Pauli paramagnetic one, whereas the susceptibility of the V3 site shows the CW behavior both above and below T_{Na}. They may be due to the reconstruction of the $3d$ band because of the change in the unit cell from $a \times b \times c$ to $a \times 2b \times c$ and the change from the random to regular potentials below T_{Na}. This may lead to a broad local band at the V2 sites and a narrow band at the V3 sites. In order to understand the MI transition in β-$Na_{0.33}V_2O_5$, we should consider the quasi-one-dimensional crystal structure along the *b* axis leading to one-dimensional nature of the electronic structure. Therefore the large nesting of the Fermi surface, resulting in a Peierls-type instability, is expected to be present. Also the superconductivity appearing under high pressures seems to take place in the system of the weakly coupled three ladders as shown in Fig. 16. Band calculations and theoretical studies of the model proposed in the present study are desired to clearly understand the mechanisms of the MI transition in β-$Na_{0.33}V_2O_5$. It is also important to clarify the CO pattern in the insulating phase. Our ^{23}Na NMR studies on the CO pattern will appear elsewhere.[21]

V. SUMMARY

We have made ^{51}V NMR measurements on a single crystal to study the local magnetic susceptibility and the electronic structure at the vanadium sites in β-$Na_{0.33}V_2O_5$. We measured the temperature dependence of the principal components of the Knight shift and the electric field gradient tensors of the V2 and V3 sites. From the bulk magnetic susceptibility and the Knight shifts we estimated local magnetic susceptibilities of the V1, V2, and V3 sites particularly in the metallic phase. We found that local magnetic susceptibility of the V1 sites is larger than those of the V2 and V3 sites in the metallic state. We also proposed a model of the electronic structure to understand electronic and magnetic properties of the metallic phase in β-$Na_{0.33}V_2O_5$.

ACKNOWLEDGMENTS

The authors would like to thank J. Yamaura, M. Isobe, S. Nagai, and T. Kozuka for fruitful discussions, and to acknowledge S. Inoue for technical support. This study was supported by a Grant-in-Aid for Scientific Research from the Japan Society for the Promotion of Science.

[1] M. Imada, A. Fujimori, and Y. Tokura, Rev. Mod. Phys. **70**, 1039 (1998).
[2] M. Isobe and Y. Ueda, J. Phys. Soc. Jpn. **65**, 1178 (1996).
[3] H. Seo and H. Fukuyama, J. Phys. Soc. Jpn. **67**, 2602 (1998).
[4] H. Yamada and Y. Ueda, J. Phys. Soc. Jpn. **68**, 2735 (1999).
[5] Y. Ueda, M. Isobe, and T. Yamauchi, J. Phys. Chem. Solids **63**, 951 (2002).
[6] A. N. Vasil'ev, V. I. Marchenko, A. I. Smirnov, S. S. Sosin, H. Yamada, and Y. Ueda, Phys. Rev. B **64**, 174403 (2001).
[7] T. Yamauchi, Y. Ueda, and N. Môri, Phys. Rev. Lett. **89**, 057002 (2002).
[8] A. D. Wadsley, Acta Crystallogr. **8**, 695 (1955).
[9] M. Itoh, N. Akimoto, H. Yamada, M. Isobe, and Y. Ueda, J. Phys. Soc. Jpn. Suppl. B **69**, 155 (2000).
[10] M. L. Doublet and M. B. Lepetit, Phys. Rev. B **71**, 075119 (2005).
[11] M. Itoh, N. Akimoto, H. Yamada, M. Isobe, and Y. Ueda, J. Phys. Chem. Solids **62**, 351 (2001).
[12] S. Nishimoto and Y. Ohta, J. Phys. Soc. Jpn. Suppl. B **70**, 309 (2001).
[13] J. Yamaura, M. Isobe, H. Yamada, T. Yamauchi, and Y. Ueda, J. Phys. Chem. Solids **63**, 957 (2002).
[14] M. Heinrich, H.-A. Krug von Nidda, R. M. Eremina, A. Loidl, Ch. Helbig, G. Obermeier, and S. Horn, Phys. Rev. Lett. **93**, 116402 (2004).
[15] K. Okazaki, A. Fujimori, T. Yamauchi, and Y. Ueda, Phys. Rev. B, **69**, 140506(R) (2004).
[16] S. Nagai, M. Nishi, K. Kakurai, Y. Oohara, H. Yoshizawa, H. Kimura, Y. Noda, B. Grenier, T. Yamauchi, J. Yamaura, M. Isobe, Y. Ueda, and K. Hirota, J. Phys. Soc. Jpn. **74**, 1297 (2005).
[17] G. M. Volkoff, H. E. Petch, and D. W. Smellie, Can. J. Phys. **30**, 270 (1952).
[18] A. Abragam, *The Principles of Nuclear Magnetism* (Clarendon, Oxford, 1961).
[19] H. Yasuoka, T. Ngwe, V. Jaccarino, and H. J. Guggenheim, Phys. Rev. **177**, 667 (1969).
[20] *International Table for Crystallography*, edited by Th. Hahn (Kluwer Academic, Dordrecht, 2002), Vol. A.
[21] M. Itoh, I. Yamauchi, T. Kozuka, T. Suzuki, T. Yamauchi, J. Yamaura, and Y. Ueda (unpublished).
[22] *Atomic and Molecular Physics*, edited by K. H. Hellwege and A. M. Hellwege, Landölt-Bornstein, New Series, Group II (Springer, Berlin, 1986), Vol. 16.
[23] T. Kiyama, H. Saitoh, M. Itoh, K. Kodama, H. Ichikawa, and J. Akimitsu, J. Phys. Soc. Jpn. **74**, 1123 (2005).
[24] A. Abragam and B. Bleaney, *Electron Paramagnetic Resonance of Transition Ions* (Clarendon, Oxford, 1970).
[25] J. Yamaura, M. Isobe, T. Yamauchi, and Y. Ueda (unpublished).
[26] J. Yamaura, T. Yamauchi, M. Isobe, H. Yamada, and Y. Ueda, J. Phys. Soc. Jpn. **73**, 914 (2004).
[27] A. C. Gossard, J. P. Remeika, T. M. Rice, H. Yasuoka, K. Kousge, and S. Kachi, Phys. Rev. B **9**, 1230 (1974).